Proceedings of the ASME 2022 17th International & Manufacturing Science and Engineering Conference MSEC 2022 June 27-July 1, 2022, West Lafayette, Indiana, USA

MSEC2022-85439

TOWARDS A DIGITAL TWIN: SIMULATION AND RESIDUAL STRESS ANALYSIS IN AEROSPACE COMPOSITE STRUCTURES ASSEMBLY

Tim Lutz
Graduate Research Assistant
Virginia Polytechnic Institute and State University
Blacksburg, Virginia 24061
Email: tlutz@vt.edu

Xiaowei Yue*
Assistant Professor
Virginia Polytechnic Institute and State University
Blacksburg, Virginia 24061
Email: xwy@vt.edu

Jaime Camelio
Professor
University of Georgia
Athens, Georgia 30602
Email: jcamelio@uga.edu

ABSTRACT

Aerospace composites assemblies/joining demand ultra-high precision due to critical safety requirements, which necessitate adherence to indicators of risk that are often difficult to quantify. This study examines one important indicator, the residual stress that arises as a result of dimensional mismatch between mating components during the composite structures assembly process. Conventional simulations of large components assemblies investigated the process at a local or global scale, but lacked detailed exploitation of multi-layer stress analysis at integrated scale for composite structures. We develop a novel digital twin simulation for joining large composite structures with mechanical fasteners. The digital twin simulation integrates global features and local features for detailed investigation of stresses. We perform a statistical analysis to better understand the numerical properties of residual stresses after the fastening. Goodness-of-Fit tests and normality tests are used to explore the probabilistic distributions of the stresses exceeding a chosen safety threshold. The case study is conducted based on composite fuselage joining. The results show the stresses in composite structures assembly follow extreme value distributions (such as Weibull, Gumbel) rather than the widely used Gaussian distribution. The stresses in joined composite structures differ across layers, which can be attributed to the anisotropic material behavior.

*Correspondence author: Dr. Xiaowei Yue (Email: xwy@vt.edu).

INTRODUCTION

In recent years, commercial aircraft manufacturers have introduced carbon fiber composites in primary structures such as the airplane fuselage and wing sections. For example, the Boeing 787 aircraft is built with at least 50% of composite materials by weight [1]. Likewise, Airbus has pushed composites with the A350 XWB which benefits from being built with 53% composite materials [2]. This trend is expected to continue - according to the American Composites Manufacturers Association, the composites industry contributes $22.2 billion to the US economy annually, and by 2022, the end-product market for composites is expected to reach $113.2 billion [3], fueling the American economy. While carbon fiber composite materials promise performance gains due to superior strength-to-weight ratio, stiffness-to-weight ratio, and corrosion-resistance when compared to metal alloys, they are also far more complex to model due to their anisotropic and nonlinear behavior. This has led to serious concerns and setbacks in the manufacturing processes. As recently as in 2020, a major airplane manufacturer reported problems with its composite fuselage production [4]. In this instance, shims manufactured to compensate dimensional variations of fuselage sections to be joined were found to be out of tolerance, which led to an investigation into if and how to rectify this error. In this problem, the residual strains and stresses in and around fasteners are difficult to characterize, and uncertainty arises when parts deviate from their nominal specifications. Yet, given the safety-critical nature of the application, it is crucial to have a solid understanding of how process devia-

Copyright © 2022 by ASME

tions impact failure criteria evaluated at the joint. This knowledge is required to properly adjust process parameters so that critical safety margins are maintained and guaranteed in the final product. While it is possible to carry out explicit finite element modeling of a given assembly, given time and labor constraints, it is infeasible to do so every time a particular assembly step is performed. Hence, an innovative method with a simpler and faster model is desired to inform decisions in the manufacturing setting.

Literature Review

There exist several families of models that are relevant for evaluating the quality of large structures in aerospace assemblies. Firstly, detailed numerical models of joint behavior are important tools for ensuring that fasteners are appropriately selected and installed for their given application. For example, a very detailed finite element model of a rivet was developed by Abdelal et al. [5]. Different rivet head designs and the effect of varying pitch distances were investigated. Yoon et al. reported on a dynamic numerical simulation that studied the installation of a rivet in a laminated composite [6]. They empirically determined an optimal maximal squeeze force by trial and error, as their computations took several hours on a supercomputer. Stocchi et al. studied countersunk fasteners under load, taking into account different clamp forces, hole clearance, and friction coefficients [7]. Their finite element model consists of two fasteners, for which they observed several stages of behavior during loading (slip, no-slip, full contact, damage, failure). Secondly, variation propagation models shed light on the deformations that result from dimensional deviations, part positioning and fixturing, and the installation of fasteners. A deviation propagation model proposed by Lin et al. condenses finite element models of compliant parts into substructures with reduced degrees of freedoms [8]. Li et al. proposed a variation propagation model for fuselage panel assembly in which they extracted a structure stiffness matrix from FEA model [9]. Cheng et al. modeled key points and control points via discretized beam connections in a finite element model [10]. They attempted to mimic an assembly process with the following steps: position, coordinate clamp forces, join, release. Wang et al. considered the effects of positioning variations of stringers on deformation of aeronautical parts in their theoretical model based on conservation of energy [11]. Zhang and Shi investigated the variation propagation modeling and developed methods to predict assembly deviation for compliant composite parts in both single-station assembly [12] and multi-station assembly [13]. Their methods consider various deviation sources including part manufacturing error, fixture position error, and relocation-induced error. A surrogate model based optimal feed-forward control strategy was further developed to reduce dimensional deviations and prevent defects [14]. Diverse uncertainty sources (including actuator uncertainty, part uncertainty, modeling uncertainty, and unquantified uncertainty) are considered in surrogate modeling [15]. All of these variation propagation focus on deformation; because of their varying approaches to reducing the model, details about what happens at locations other than designated points of interest are lost in the analysis. Thus, the two aforementioned families of models represent models at a local and a global scale, respectively.

In the context of large assemblies with many fasteners, the local and global scales must be bridged in order to convey a full picture of the assembly process. Often times, this is addressed via a local-to-global approach wherein a simplified model of a fastener is proposed and experimentally calibrated or verified. Then, distortions arising from multiple fastener installations are calculated. Masters et al. modeled local distortions around a self-piercing rivet, then used this local model to predict global distortions due to the fastener installation [16]. By converting a dynamic numerical model of the rivet installation process into boundary conditions in a static model, Ni et al. investigated the effect of fastening sequence in an antenna assembly [17]. Yang et al. proposed a rivet equivalent unit, an algebraic model that takes into account the deformation of the rivet during installation [18]. Wang et al. and Zheng et al. also proposed a rivet equivalent units for the expansion of rivets during installation [19] [20]. We note that none of these works consider composite structures, but rather installation of fasteners in aluminum components. They generally focus on the effects of rivet expansion during installation, and not mismatch of assembly component dimensions.

While many of the aforementioned studies focus on deformation, they do not place much emphasis on evaluating characteristics related to failure of the joints.There are a number of studies that have seek to understand the failure mechanisms of fasteners in aerospace applications. Some researchers aimed to predict the fatigue life of riveted joints in aerospace structures [21, 22]. They identified localized stresses were an important factor in joint failure. This observation is consistent with Thoppul et al.'s overview of failures in mechanically fastened composite joints [23].

The above works represent detailed studies on a relatively small number of fasteners in a simple geometry. Studies of parts under load consider stresses only on a local scale. They do not capture the effects of residual stresses due to geometrical variations of large parts. Towards this end, Wen et al. developed a simulation model residual stresses due to dimensional variations of composite fuselage sections that are being joined together [24]. A similar study can be found in [25] where a wing box was used as a case study. While here, macroscopic/global effects were investigated, fasteners were not explicitly modeled in the simulation. In contrast, Askri et al. considered effects geometrical variations on a bolted structure [26], but again only demonstrated results for a small structure with four bolts.

Our Contributions

Our contributions can be summarized into three aspects:

Simulation model: We build a finite element based digital twin

Copyright © 2022 by ASME

simulation of a large composite structure that integrates localized effects of fasteners and global shape deviations. Multi-scale features are fused to realize accurate simulation results.

Parametric study: We introduce geometrical deviations from nominal dimensions and observe stress/strain in the composite structure. We mimic imperfections of real-world components that are to be assembled, and calculate critical quality measures of the final assembly.

Statistical analysis: We show that maximum stress values do not follow Gaussian distributions, but rather extreme-value distributions. We conduct a statistical analysis that characterizes the probability of exceeding safety critical thresholds for a given set of input parameters.

DIGITAL TWIN SIMULATION DEVELOPMENT

Experimental investigation for composites assembly tends to be extremely expensive and time-consuming. This is especially true for large structures as are common in aerospace applications. Computational simulations can provide a more flexible tool for early-stage technology development and methodology proof-of-concept. We build a digital twin simulation for investigating the effects of shape variations of components in a composite assembly on failure criteria. It consists of (1) a parametric geometry design, i.e., computer-aided design (CAD), (2) modeling of the composite layup structure, and (3) a finite element model to exactly mimic the composite structures assembly. In a production setting, critical dimensions of fuselage components may be collected upstream (e.g., via laser metrology), prior to when parts are to be joined. With this data, our model may be leveraged to pre-compute failure criteria given actual part dimensions, and to then inform production personnel whether or not countermeasures such as fabricating shims are necessary. In current practice, such information is not readily available on the shop floor. While this digital twin scheme does not synchronously mirror all sub-steps of the assembly process, it can provide critical information at discrete time steps during the fuselage joining stage.

Geometry of the Components

We develop a finite element model of a composite airplane fuselage skin, which is to be joined to an inner support at the boundary to a second fuselage section. A total of 864 fasteners in alternating rows are defined for the connection. The fuselage barrel represents an "imperfect" cylinder, which is fixed at the far end opposite to the joint. Though we could vary the shape of the inner support as well, it is taken to have a perfect circular cross-section in order to limit the number of parameters that define the model. The overall length of the fuselage section is 2m, as is its nominal diameter. The thickness of the fuselage skin is 5mm. A rendering of the geometry created in the CAD software is shown in Fig. 1 .

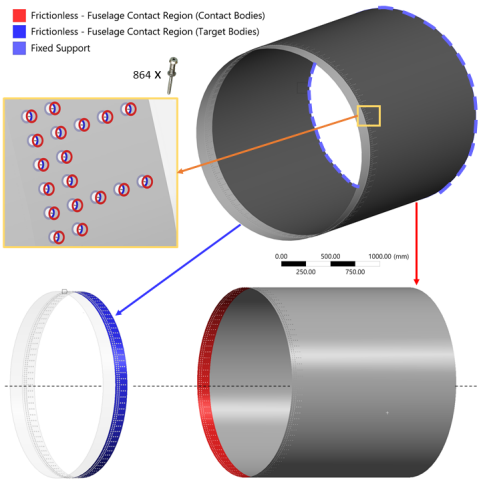

FIGURE 1. Simplified geometry of the fuselage used for the finite element simulation. There are 864 fasteners, which are modeled as spring connections. The edge at the far end of the fuselage is fixed. An exploded view of the components is shown at the bottom, along with the contact surfaces. Contacts between the components are modeled as frictionless.

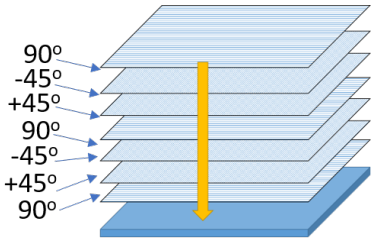

FIGURE 2. One ply design in carbon fiber reinforced composite.

Material Structures of Carbon Fiber Reinforced Composite

We build a composite structure comprised of multiple layers of fabric with a given thickness and orientation. By orientation, we refer to the direction in which fibers are aligned inside the laminate relative to a reference coordinate frame on a given face of the part. This is to mimic the physical process in which multiple layers of fabric are draped over one another, following a prescribed layup sequence, as shown in Fig. 2 [27]. Imperfections in this process such as bubbles and wrinkling of the fabric are not considered in our model.

As defined in ANSYS ACP PrepPost, our fuselage is made up of multiple sublaminates, each consisting of five layers of unidirectional carbon fiber prepreg fabric. The layers are oriented at $[0°, -45°, 90°, 45°, 0°]$ angles, respectively. Here, 0 degrees corresponds to the direction along the circumference of the cylinder. A single layer is 0.2mm thick, resulting in a total thickness of

Copyright © 2022 by ASME

5mm. This layup pattern is similar to a quasi-isotropic pattern, but it does maintain anisotropic behavior. In the real world example we use as a reference, carbon fiber layers are applied onto a mandrel via continuous fiber placement. The placement of layers is proprietary to the manufacturer.

Polar plots Fig. 3 and 4 specifically illustrate the directional stiffnesses in all directions relative to the reference angle of the layers. The left-hand side of the plot illustrates the layup schedule of the overall laminate and individual stackups, respectively. In these plots, an isotropic material would exhibit perfect circles for E1, E2, and G12. While the bulk laminate exhibits mildly anisotropic behavior, the stackup layers from which it is constructed have much more isotropic polar properties. It is necessary to individually inspect these layers to understand failure mechanisms.

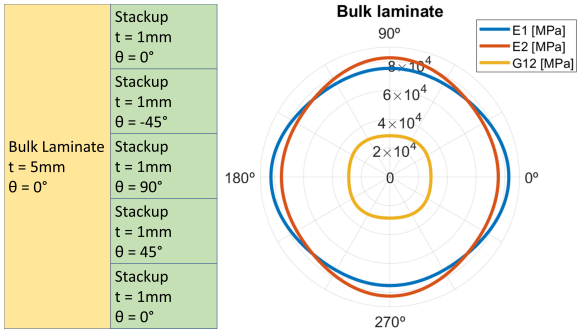

FIGURE 3. Engineering constants for our bulk carbon fiber reinforced composite laminate. It features five stackups at angles $[0°, -45°, 90°, 45°, 0°]$ as defined in Fig.

4 below. While the bulk properties are close to isotropic, sub-analysis of the anisotropic individual stackup components is crucial for modeling failures.

Laminate Theory and Adjustments in Simulation

The composite structure is passed into the FEA analysis software as a shell model. Here, we define boundary conditions including supports, connections, and surface contacts. Inside the FEA software, the composite structure is treated according to Classical Laminate Theory (CLT) [28, 29], which relies on a number of underlying assumptions. These include: perfectly bonded layers, uniform material properties through each respective layer, linear-elastic stress-strain behavior, plane stress state, relatively small curvature of the part, and relatively small in-plane strains. These assumptions are generally satisfied when the wall thicknesses of a part are small relative to the overall extents of the part.

CLT calculates the strain at a distance z away from the middle surface by taking the strains at the middle surface $\boldsymbol{\varepsilon^0}$, $\boldsymbol{\gamma^0}$ and

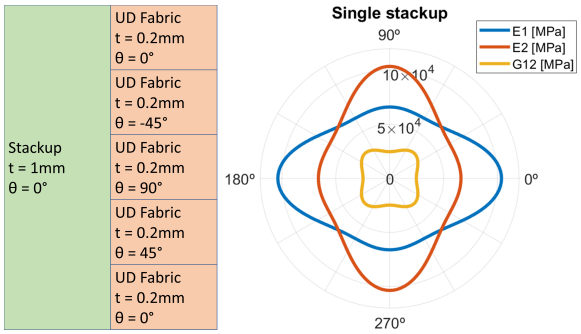

FIGURE 4. Engineering constants for a simple carbon fiber composite stackup featuring five unidirectional fabric layers at angles $[0°, -45°, 90°, 45°, 0°]$. This stackup exhibits anisotropy, i.e., a strong variation of E1, E2 and G12 with respect to angle.

considering in the middle surface curvature $\boldsymbol{\kappa}$:

$$\boldsymbol{\varepsilon} = \begin{bmatrix} \varepsilon_x \\ \varepsilon_y \\ \gamma_{xy} \end{bmatrix} = \begin{bmatrix} \varepsilon_x^0 \\ \varepsilon_y^0 \\ \gamma_{xy}^0 \end{bmatrix} + z \begin{bmatrix} \kappa_x \\ \kappa_y \\ \kappa_{xy} \end{bmatrix} = \boldsymbol{\varepsilon^0} + z\boldsymbol{\kappa}. \tag{1}$$

For a flat plate, $\kappa_x = \frac{\partial^2 w_0}{\partial x^2}$, $\kappa_y = \frac{\partial^2 w_0}{\partial y^2}$, and $\kappa_{xy} = 2\frac{\partial^2 w_0}{\partial x \partial y}$. The terms κ_x and κ_y correspond curvature due to bending, while κ_{xy} is due to twist. For a more complex shape, a more complicated expression will have to be derived from the appropriate strain-displacement relationship. That means the correlations among multiple layers/plies of laminate are considered.

At this point, we would like to note that even though engineering constants including the Young's moduli in the 0° and 90° directions of the laminate, E_1 and E_2, the in-plane shear stress G_{12}, and the bulk modulus η_{12} can be derived from the stiffness matrix (or its inverse, the compliance matrix), an analysis that simply relies on these engineering constants can fail to capture the coupling effects that are present in a laminate structure. Nonetheless, these engineering constants are useful measures for illustrating the anisotropic material properties of a laminate composite structure, as shown in Fig. 3 and Fig. 4.

Fastener Model

In order to model a large number of rivet lap joints in the assembly, we introduce an approximation for fasteners to keep computational requirements within reasonable bounds. Our approximation of a solid rivet is to insert a stiff spring element between faces corresponding to the rivet head contact areas. Once installed, a solid rivet should really be considered to be a very stiff spring [30]. For this reason, we choose to model the installation procedure by directly setting the initial free length of the spring. By taking into account the thicknesses of the components to be

Copyright © 2022 by ASME

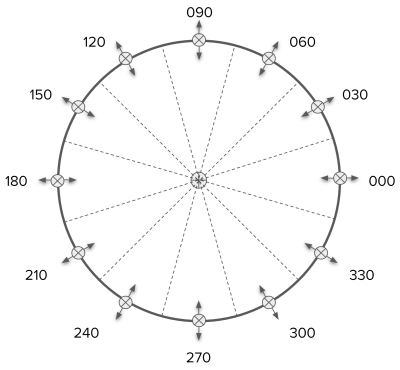

FIGURE 5. Radial deviations at the 12 spline control nodes are evenly spaced around the circumference of the fuselage. Dashed lines correspond to subregion boundaries.

joined, the mating surfaces can be adjusted to touch (or to maintain a very small gap within the tolerance). In this way, direct contact between the components can be enforced as an initial condition. We assume that the components alignment has been accomplished via a shape control mechanism as described in [15].

An approximate spring stiffness can be derived from the stress-strain relationship of a uniform bar under tension as follows. Consider a fastener with cross-sectional area A and length L. Given the Young's modulus E of the material the fastener is made of, the change in length in response to a force F is $\Delta L = \varepsilon L = \frac{FL}{AE}$. Rearranging and comparing this expression to Hooke's Law $F = k\Delta L$, the spring stiffness is then given by $k = \frac{AE}{L}$. We use this expression to estimate a spring stiffness for the fasteners used in our finite element model, choosing parameters based on dimensions and materials of typical aerospace fasteners. Specifically, we base our calculations on grade 5 titanium (Ti 6Al-4V) fasteners, which are preferred for installations in composite parts.

Parametric Computer-aided Design

We integrate a parametric CAD model with a finite element analysis to study the residual stresses (and other failure criteria) that result from geometrical variations of composite structures joined together with fasteners. In this study, we introduce shape deviations by parameterizing the underlying geometry in the CAD model. At the root of the geometry is a spline curve defined by 12 points on a circle (see Fig. 5), which we extrude into a roughly cylindrical shape corresponding to the fuselage skin. For each underlying spline point, a radial deviation from the base radius is used as an input parameter to the model.

For each parameter set, the geometry is regenerated inside the CAD software and passed into the FEA software. There, the finite element mesh is created anew from scratch, introducing some uncertainty into the results. We found that the size of the mesh parameters may affect the maximum stress values slightly. To counter this, we implemented mesh controls such as edge sizing and inflation around rivet holes in order to keep the mesh size consistent and repeatable across simulation runs. Prompted by this observation, we investigate the repeatability of our solutions over multiple regenerations of the finite element mesh.

Design of Experiment

The design of experiment is set up to span deviations in the range of (-3mm, +7mm) at every point, where a positive value corresponds to an increase in the nominal radius of 1000mm. The Latin Hypercube design for generating simulation points results in a space-filling design [31]. This is desirable from a perspective of how much information can be gained from each simulation run. Here, we focus on one-shot design of experiment. For sequential design or iterative experimentation, please refer to [32, 33]. We assume that radial displacements are close to uniformly distributed for each of the 12 control nodes. The mean of radial displacements in this design is equal to the centerpoint of the possible deviations, which is +2mm. In total, 91 design points were chosen.

SIMULATION RESULTS AND DISCUSSION

Equivalent Stress

Equivalent stress, also referred to as Von-Mises stress, provides a scalar measure that combines the nine individual components of the stress tensor into a single value. As such, it is a easily visualized in heat maps as in Fig. 6. During the assembly process, stresses occur in response to forces applied by fixtures, tools, and fasteners. In the interest of identifying where the largest stresses occur during the assembly process, equivalent stress is an appropriate metric to be used for identifying problem regions.

In our simulation results, we observe that average equivalent stress inside the assembly tends to increase as the mean of radial deviations increases. The location of maximum equivalent stress most often is in the vicinity of the control node with the largest radial deviation. Furthermore, stresses tend to concentrate near fastener holes. Because of this, we focus our attention to the results recorded inside the interface region between the inner support structure and the fuselage skin on the outside, i.e., what we refer to as the "contact region." For the 88 sets of input parameters, on average the maximum equivalent stress was calculated at 1186MPa. Across simulations, maximum equivalent stress values span from 326MPa to 1920MPa. To aid with our subsequent analysis, we split the contact region into 12 subregions, each of which is centered on one of the twelve control points. The results recorded for these regions simply represent a subset of the results recorded for the entire contact region.

Copyright © 2022 by ASME

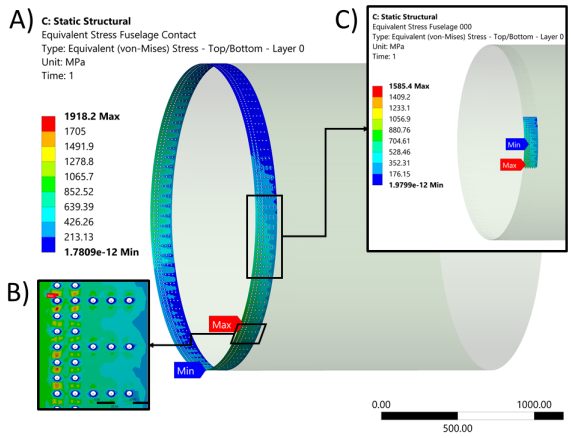

FIGURE 6. A) FEA simulation results for residual stress inside the fuselage contact region. B) The maximum stress tends to concentrate near fastener holes inside the subregion with the largest deviation from the nominal radial distance to the center axis of the fuselage. C) subregion 000, corresponding to the region centered at 0° on the circumference of the fuselage.

Repeatability Test of Digital Twin Simulation

The size of the mesh can have an significant influence on the FEA solution results. After all, the mesh size controls the granularity of results, and if the mesh is too large, extreme values that occur in small regions will be averaged out. We implement edge size and inflation controls during mesh generation, for sake of consistency between model updates and to ensure a sufficiently fine resolution of the mesh around the fastener holes, where stress tends to concentrate. To test the repeatability of our solutions, we note that our geometry definition has a 12-fold symmetry and solve for all 12 variations of the equivalent boundary conditions. Fig. 7 shows a boxplot in which the repeatability results for two different variation patterns are illustrated. We find a mean absolute percentage error from the observed mean of only 1%. Thus, we conclude that the results are close enough together that we feel confident to proceed with our analysis.

Individual Layer Stress Distributions

Given that unidirectional carbon fiber fabrics are stiffest in their principal direction, we may postulate that some fabric layers will take on more stress than others. Indeed, we observe that equivalent stress varies across different layers based on the orientation of the fabrics. The stress heatmaps in Fig. 8 illustrate that both the pattern and magnitude of stress depend on the layup angle. For fabrics places at angles that are alike, e.g., layers 1 and 5, stress values are very similar. Because our shape variations are radial displacements from a circular base, the dimensional mismatch in our model leads to hoop stress, i.e., stress around the circumference of the fuselage. The 0° direction of layers 1 and 5

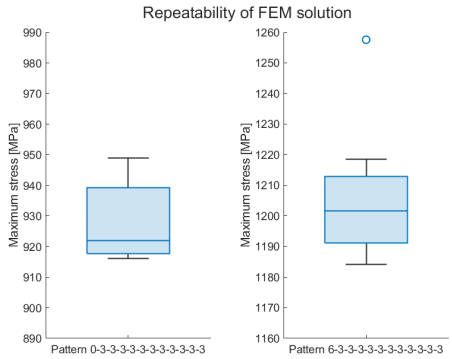

FIGURE 7. Repeatability of the FEA solution. For the first pattern, the maximum stress observed has a mean of 928MPa with a standard deviation of 12.2MPa. The second patter exhibits a mean of 1,205MPa and standard deviation of 20.0MPa. In both cases, the mean average percentage error is around 1%, respectively

aligns with this direction, so we expect these layers to experience higher stresses than fabrics at other angles. Our results show that these 0° layers do in fact experience higher stress levels than the layers placed at +/-45° or 90°.

Taking a closer look at the histograms in Fig. 8, we see that the stress distributions are multimodal, i.e., they exhibit multiple peaks. We know that stresses tend to concentrate near edges and corners. Hence, one explanation for the multimodal behavior may be that finite element nodes that are near geometric features such as the fastener holes have a different stress response (conditional probability distribution) to the fastening process than those further away. Another perspective is to look at the different subregions, some of which have larger local deviations than others. The local deviation is the biggest (though not only) driver of stress inside a particular subregion. Put more broadly, proximity of a particular node to the source of dimensional deviation is a factor in its stress response.

Interestingly, if we scale the observed stress values inside these particular subregions by the inverse of mean stress observed therein, we consistently recover a near identical distribution within a single simulation. Furthermore, this holds true when we consider results from other simulation runs with different input parameters. In fact, when we apply deviations that are equal at all positions, the entire stress distribution follows this pattern.

STATISTICAL ANALYSIS

In this section, we conduct statistical analysis in the context of considering maximum equivalent stress values observed across all simulation runs. From this perspective, we aim to deduce insights about residual stresses from the effect of part-to-part variation, such as relationships between input and output parameters of the fastening process.

Copyright © 2022 by ASME

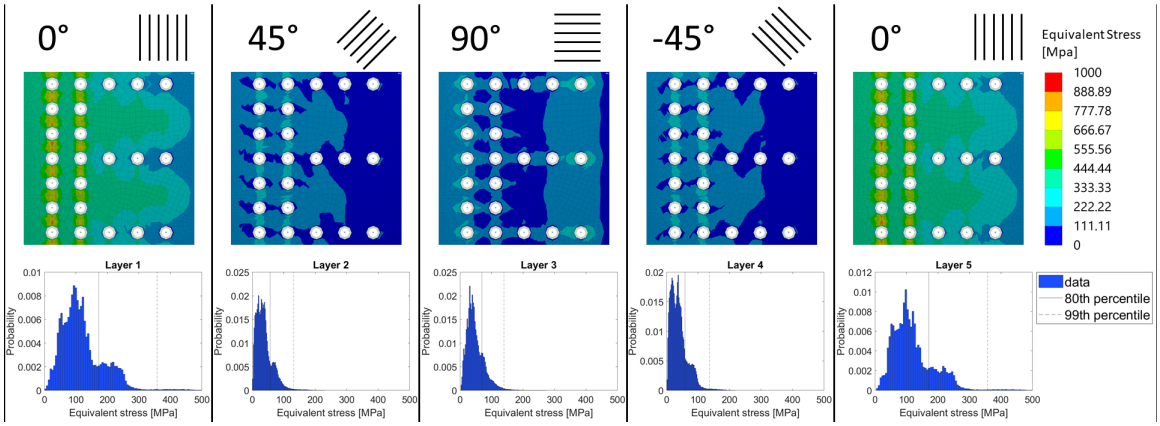

FIGURE 8. Equivalent stress inside the first five unidirectional carbon fiber layers of the fuselage skin. The detail heat maps indicate that stress differs across layers, which can be attributed to anisotropic material behavior. The histograms show distributions of single layer stress values taken from the entire contact region of the fuselage.

Extreme Value Theory

In the context of failure criteria, concerns arise when a quantity of interest (e.g., stress) exceeds a certain threshold. One critical research question is: given the information at hand, what is the probability that a safety threshold is being surpassed? In many engineering examples, the answer to this question is driven by how structures behave in small regions where failure may occur. Many popular statistical techniques center around predicting the mean of a distribution that would encompass the behavior of the entire structure. For this purpose, we can rely on the Central Limit Theorem (CLT) as a powerful tool. However, the detailed dynamics in the small regions of interest can be viewed as "rare" events inside the structure at large. As such, to apply statistical methods that focus on the mean of the distribution is not a good approach. Rather, it is prudent to characterize the behavior at the tail of the distribution. Extreme value theory (EVT) represents a branch of statistics that provides the tools for doing so [34]. In a sense, EVT provides an analogue to the CLT for extreme values.

At the core of EVT stands the Fisher-Tippett-Gnedenko theorem [35], which states when a given sample of independent and identically-distributed (i.i.d.) random variables undergoes an appropriate scale and shift operation, the probability distribution of the sample maxima will asymptotically approach the generalized extreme value distribution (GEV). Formally, the extremal types theorem can be stated as follows. Let $X_1,...,X_n$ be a series of i.i.d. random variables and let $M_n = \max\{X_1,...,X_n\}$. If there exist series of constants $\{a_n\}$ and $\{b_n\}$ such that

$$\Pr\left\{\frac{M_n - b_n}{a_n} \leq z\right\} \to G(z) \text{ as } n \to \infty,$$

then $G(z)$ will converge in distribution to the GEV distribution. This distribution is fully specified by the extreme value index γ, location parameter μ, scale parameter σ, and shape parameter ξ via the following expression [36]:

$$G(z) = \exp\left[-\exp\left\{1-\xi\left(\frac{z-\mu}{\sigma}\right)\right\}^{-1/\xi}\right]. \qquad (2)$$

It is defined on $z:\ 1+\xi(z-\mu)/\sigma > 0$ and valid parameters are $-\infty < \mu < \infty$, $\sigma > 0$, and $-\infty < \xi < \infty$. Remarkably, the GEV distribution in fact unifies three otherwise known distribution families, which are often referred to as extreme value distributions of type I,II,III. By name, they are known as (I) Gumbel ($\xi \to 0$), (II) Fréchet ($\xi > 0$), and (III) Weibull ($\xi < 0$). For, replacing $1/\xi$ with $\alpha > 0$ in equation (2), we get the familiar expressions. In particular, the Weibull distribution (III) frequently occurs in reliability applications.

By statistical analysis, we find that if we consider the maximum Von-Mises stress values observed across all our simulation runs are better approximated with an extreme value distribution than a normal distribution, as indicated by Fig. 9.

Threshold Exceedance

In a production setting, it is prudent to set a limit for the maximum allowable residual stress resulting from the dimensional mismatch of components. This is necessary in order to assemble a final product that fulfills its safety requirements. In effect, this would correspond to looking at the tail of the distribution shown in Fig. 9. We split the results into twelve subregions centered around the twelve spline nodes driving the deformation of the fuselage skin and consider the maximum stress observed in these subregions. To investigate the pattern of stresses exceeding safety threshold, we use quantile regression to fit the data from each subregion. In Fig. 10(a), we show the quantile regression

Copyright © 2022 by ASME

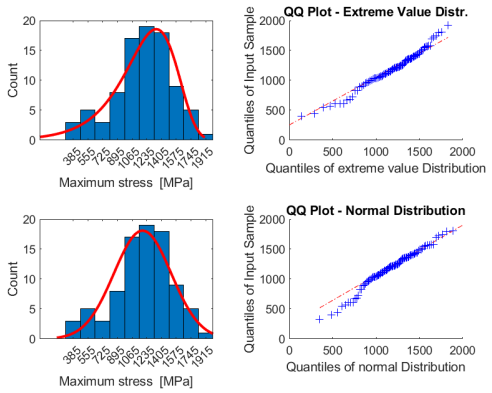

FIGURE 9. Comparing extreme value and normal distribution fits for Von Mises maximum stress values across all simulation runs inside the 0° subregion.

fit with a 2nd order polynomial for the 95th percentile of our data along with 95% confidence intervals for the predictions. Confidence bounds for the resulting predictions can be estimated via bootstrapping. From Fig. 10(a), we can see that maximum stress inside a subregion tends to increase as the radial deviation in that region increases. Closing the gap between the inner and outer components during fastening leads to strain and thus stress in the assembly. Using quantile regression, the fitted τ-quantile line for $\tau = 0.95$ provides a clearer indication as to whether the assembly can be considered safe. Once we have obtained an estimate for a τ-quantile, we can claim with some quantifiable confidence that a fraction of $(1-\tau)$ values will exceed the estimated curve. In the absence of heteroscedasticity, we may further characterize a probability distribution by investigating the exceedance values, using the τ-quantile curve as a threshold, which is conditional upon the radial deviation inside the subregion of interest. Thereby, we can provide a conditional probability that a fixed threshold is going to be exceeded. This can be accomplished by looking at the distance between the quantile regression prediction at a given radial deviation and the fixed threshold, and calculating the tail probabilities according to the fitted distribution of values above τ-quantile line.

For output data y, let $\hat{y}_\tau$ be the τ-quantile value predicted from the quantile regression model for a given input x. Consider the distance d to a fixed threshold C, i.e., $d(x) = C - \hat{y}_\tau(x)$. Suppose the exceedance values $\rho = y - \hat{y}_\tau$, $\rho > 0$ follow a known distribution characterized by a cumulative density function $F(\rho)$. Suppose the values y are homoscedastic, which implies the distribution of exceedance values, $F(\rho)$, is independent of x. When $d > 0$, the probability that given x, the observed output y exceeds the chosen threshold C can be calculated as $P(y > C|x) = (1 - F(d(x))(1-\tau)$.

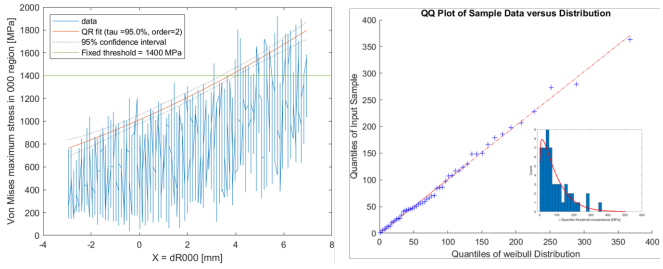

FIGURE 10. (a) τ-quantile regression fit for $\tau = 0.95$ with confidence bounds calculated via a bootstrap; (b) QQ plot of the values of maximum Von-Mises stress exceedance values above the 95th percentile regression line against a fitted Weibull distribution (0° subregion).

Statistical Goodness-of-Fit Test

We conduct statistical Goodness-of-Fit test based on the simulation data. We find that both a Weibull or a generalized Pareto distribution adequately fit the exceedance data. quantile-quantile (QQ) plot for the Weibull distribution in Fig. 10(b) shows that the exceedance data follows a Weibull distribution. In contrast to probability plots, goodness-of-fit tests offer a measure to objectively reject that a sample was drawn from a supposed underlying distribution function. Supposing that a set of observations is drawn from an underlying distribution function, there exist several quantitative goodness-of-fit tests that may reject that hypothesis based on a calculated score. These include the Kolmogorov-Smirnov (KS) test, Lilliefors test, Anderson-Darling test, Cramer-Von Mises test, Shapiro-Wilk test, Shapiro-Francia test, Jarque-Bera test, and D'Agostino-Pearson test [37, 38].

In Table 1, it is evident that all but the KS test reject the assumption that the maximum stress values above the τ-threshold ($\tau = 0.95$) follow a normal distribution at the 1% level. KS test cannot reject the normality hypothesis. One explanation is that KS test is more sensitive to the center of a distribution than at its tails, hence it does not perform well for exceedance data. The Anderson-Darling test is an improvement over the KS test as it adapts critical values based on the distribution to be tested. The Anderson-Darling test is more sensitive to the tail behavior of a sample than the KS test.

The Anderson-Darling test is based on the test statistic

$$A^2 = -n - \sum_{i=1}^{n} \frac{2i-1}{n} \left[\log F_0(X_i) + \log(1 - F_0(X_{x+1-i}))\right] \quad (3)$$

where $\{X_1 < ... < X_n\}$ are ordered sample data and $F_0(X)$ is the postulated cumulative density function. The test statistic A^2 is to be compared against a critical value that depends on the postulated distribution. When the test statistic A^2 is greater than the critical level for a chosen significance level α, the hypothesis that the data are distributed as $F_0(X)$ is rejected. In Table 2, we report

Copyright © 2022 by ASME

Normality test	Reject H_0	Test statistic	p-value
KS	No	1.256	0.0944
Lilliefors	Yes	0.1714	0.0006
Anderson Darling	Yes	2.1055	0.0001
Cramer-Von Mises	Yes	0.3586	0.0001
Shapiro-Wilk	Yes	0.8676	0.0000
Shapiro-Francia	Yes	0.8670	0.0001
Jarque-Bera	Yes	21.5204	0.0000
D'Agostino-Pearson	Yes	17.8135	0.0001

TABLE 1. Statistical Goodness-of-Fit test results for exceedance data.

Distribution	Reject H_0	p-value	A^2	CV
Normal	Yes	0.0005*	2.0738	0.7404
Gumbel	Yes	0.0005*	3.8817	0.7482
Weibull	No	0.9900	0.1242	0.7482
GP	No	0.9978	0.1600	2.4974
GEV	No	0.9598	0.2683	2.4974

TABLE 2. Anderson-Darling test statistics on data exceeding 95%-quantile threshold for a significance level $\alpha = 0.05$. (*) Indicates that the true p-value is smaller than the smallest tabulated value of 0.0005.

Anderson-Darling test results for extreme value type distribution assumptions. The Anderson-Darling test rejects a normal distribution fit, while returning favorable p-values for the Weibull and generalized Pareto distributions, as well as the generalized extreme value distribution. For the two-parameter Weibull fit (which assumes the location parameter $\mu = 0$), the fitted shape parameter is $\alpha = 1/\xi = 94.0203$ and the scale parameter is $\sigma = 1.12733$.

Calculation of Exceedance Probabilities

We apply our proposed method for evaluating the probability of maximum equivalent stress values exceeding a chosen threshold to our simulation dataset. To provide an illustrative example, let us choose a hypothetical threshold $C = 1400$MPa. Based on this choice for C, Table 3 provides estimates of threshold exceedance probabilities for local radial deviations δr ranging from 0mm to 4mm. As the magnitude of local deviation increases, the risk of exceeding the threshold value increases. Based on the acceptable level of risk, these calculated probabilities may inform operators to when corrective measures should be taken during the assembly process. For example, if the probability of maximum equivalent stress to exceed our chosen threshold by more than 2 per thousand, a shim may need to be installed to close the gap between the inner and outer surfaces of the assembly components. In practice, different choices for C and acceptable exceedance probabilities may be dictated by engineering requirements.

δr [mm]	$\hat{y}_{0.95}(\delta r)$ [MPa]	d [MPa]	$P(y > C\|\delta r)[\%]$
0.0	1013.1	386.9	0.04
0.5	1060.1	339.9	0.07
1.0	1108.6	291.4	0.14
1.0	1158.6	241.4	0.28
2.0	1210.1	189.9	0.55
2.5	1263.0	137.0	1.08
3.0	1317.4	82.6	2.11

TABLE 3. Calculated probabilities of maximum equivalent stress inside a subregion to exceed a hypothetical threshold $C = 1400$MPa in response to radial deviations δr

CONCLUSION

We introduced a digital twin simulation for assembling a large composite aerospace structure. The analysis takes into account anisotropic material behavior of the composite laminate. The finite element model features a large number of fasteners (864 fasteners) that are approximated as springs. We report equivalent stress values for the regions of interest around the joints, and provide results at the individual layer level. We found that depending on the orientation of the principal directions of the lamina, the stress distribution differs across the layers in the composite laminate.

In a parametric study, we investigated the effects of deviations of the assembly from nominal dimensions on residual stresses that arise from fastening the components. In practice, the input parameters to this simulation could be linked up with physical measurements collected during production (e.g., laser metrology). By doing so, a digital twinning can be achieved at discrete time steps during the assembly process.

Statistical Goodness-of-Fit tests showed the stress data follows extreme value distributions rather than Gaussian distributions. Taking this into account, we performed a statistical analysis in which we utilized extreme value theory and quantile regression in order to quantify the probability of maximum stress exceeding a chosen threshold, conditional upon the local dimensional deviation inside the subregion of interest. The calculation can be performed on-the-fly to quickly determine the present level of risk of the assembly. Given a favorable result, assembly may proceed without intervention. Otherwise, the determined risk level may motivate computations with a higher-fidelity simulation

Copyright © 2022 by ASME

model such as the one we developed, to further determine what countermeasures may be necessary.

Implementation Notes

In our implementation, the geometry is defined in Siemens NX 12.0, while the composite model and finite element model reside within ANSYS Workbench 2020 R2. We bridge the two software packages with the CAD Configuration Manager available from ANSYS. All our computations were performed on an 8th Generation Intel Pentium Core I7 CPU with six cores and 16GB RAM. A single simulation run completed in around 1.5 hours.

ACKNOWLEDGMENT

This publication is based upon work supported by the National Science Foundation under Grant No. 2035038, and work supported by The Grainger Foundation Frontiers of Engineering Grants Program of the National Academy of Engineering. Thanks to Jeffrey H. Hunt at The Boeing Company for helpful discussions and insights.

REFERENCES

[1] Boeing. *Advanced Composite Use*. URL: https://www.boeing.com/commercial/787/by-design/. (accessed: 09/03/2021).

[2] Airbus. *A350 : the most modern and efficient aircraft*. URL: https://www.airbus.com/aircraft/passenger-aircraft/a350xwb-family.html. (accessed: 09/03/2021).

[3] American Composites Manufacturers Association. *Composites by the Numbers*. URL: https://acmanet.org/composites-industry-overview/. (accessed: 09/03/2021).

[4] Sloan, J. *Boeing conducts inspections of 787 composite inner fuselage skin*. URL: https://www.compositesworld.com/news/boeing-conducts-inspections-of-787-composite-inner-fuselage-skin. (accessed: 09/03/2021).

[5] Abdelal, G. F., Georgiou, G., Cooper, J., Robotham, A., Levers, A., and Lunt, P., 2015. "Numerical and experimental investigation of aircraft panel deformations during riveting process". *Journal of Manufacturing Science and Engineering,* ***137***(1).

[6] Yoon, T. H., and Kim, S. J., 2011. "Refined numerical simulation of three-dimensional riveting in laminated composites". *Journal of Aircraft,* ***48***(4), pp. 1434–1443.

[7] Stocchi, C., Robinson, P., and Pinho, S., 2013. "A detailed finite element investigation of composite bolted joints with countersunk fasteners". *Composites Part A: Applied Science and Manufacturing,* ***52***, pp. 143–150.

[8] Lin, J., Jin, S., Zheng, C., Li, Z., and Liu, Y., 2014. "Compliant assembly variation analysis of aeronautical panels using unified substructures with consideration of identical parts". *Computer-Aided Design,* ***57***, pp. 29–40.

[9] Li, Y., Zhao, Y., Yu, H., and Lai, X., 2018. "Compliant assembly variation analysis of sheet metal with shape errors based on primitive deformation patterns". *Proceedings of the Institution of Mechanical Engineers, Part C: Journal of Mechanical Engineering Science,* ***232***(13), pp. 2334–2351.

[10] Cheng, L., Wang, Q., Li, J., and Ke, Y., 2015. "Variation modeling for fuselage structures in large aircraft digital assembly". *Assembly Automation*.

[11] Wang, Q., Hou, R., Li, J., Ke, Y., Maropoulos, P. G., and Zhang, X., 2018. "Positioning variation modeling for aircraft panels assembly based on elastic deformation theory". *Proceedings of the Institution of Mechanical Engineers, Part B: Journal of Engineering Manufacture,* ***232***(14), pp. 2592–2604.

[12] Zhang, T., and Shi, J., 2016. "Stream of variation modeling and analysis for compliant composite part assembly—part i: Single-station processes". *Journal of Manufacturing Science and Engineering,* ***138***(12), p. 121003.

[13] Zhang, T., and Shi, J., 2016. "Stream of variation modeling and analysis for compliant composite part assembly—part ii: Multistation processes". *Journal of Manufacturing Science and Engineering,* ***138***(12).

[14] Yue, X., and Shi, J., 2018. "Surrogate model–based optimal feed-forward control for dimensional-variation reduction in composite parts' assembly processes". *Journal of Quality Technology,* ***50***(3), pp. 279–289.

[15] Yue, X., Wen, Y., Hunt, J. H., and Shi, J., 2018. "Surrogate model-based control considering uncertainties for composite fuselage assembly". *Journal of Manufacturing Science and Engineering, Transactions of the ASME*.

[16] Masters, I., Fan, X., Roy, R., and Williams, D., 2012. "Modelling distortion induced in an assembly by the self piercing rivet process". *Proceedings of the Institution of Mechanical Engineers, Part B: Journal of Engineering Manufacture,* ***226***(2), pp. 300–312.

[17] Ni, J., Tang, W., Xing, Y., Ben, K., and Li, M., 2016. "A local-to-global dimensional error calculation framework for the riveted assembly using finite-element analysis". *Journal of Manufacturing Science and Engineering,* ***138***(3).

[18] Yang, D., Qu, W., and Ke, Y., 2019. "Local-global method to predict distortion of aircraft panel caused in automated riveting process". *Assembly Automation*.

[19] Wang, H., 2014. "Riveting sequence study of horizontal stabilizer assembly using finite-element analysis and riveting equivalent unit". *Journal of Aerospace Engineering,* ***27***(6), p. 04014040.

[20] Zheng, B., Yu, H., and Lai, X., 2017. "Assembly deformation prediction of riveted panels by using equivalent mechanical model of riveting process.". *International Journal of Advanced Manufacturing Technology,* ***92***.

Copyright © 2022 by ASME

[21] Zheng, B., Yu, H., Lai, X., and Lin, Z., 2016. "Analysis of residual stresses induced by riveting process and fatigue life prediction". *Journal of Aircraft,* ***53***(5), pp. 1431–1438.
[22] Skorupa, M., Machniewicz, T., Skorupa, A., and Korbel, A., 2017. "Fatigue life predictions for riveted lap joints". *International Journal of Fatigue,* ***94***, pp. 41–57.
[23] Thoppul, S. D., Finegan, J., and Gibson, R. F., 2009. "Mechanics of mechanically fastened joints in polymer–matrix composite structures–a review". *Composites Science and Technology,* ***69***(3-4), pp. 301–329.
[24] Wen, Y., Yue, X., Hunt, J. H., and Shi, J., 2019. "Virtual assembly and residual stress analysis for the composite fuselage assembly process". *Journal of Manufacturing Systems,* ***52***, pp. 55–62.
[25] Söderberg, R., Wärmefjord, K., and Lindkvist, L., 2015. "Variation simulation of stress during assembly of composite parts". *CIRP Annals,* ***64***(1), pp. 17–20.
[26] Askri, R., Bois, C., Wargnier, H., and Gayton, N., 2018. "Tolerance synthesis of fastened metal-composite joints based on probabilistic and worst-case approaches". *Computer-Aided Design,* ***100***, pp. 39–51.
[27] Wen, Y., Yue, X., Hunt, J. H., and Shi, J., 2018. "Feasibility analysis of composite fuselage shape control via finite element analysis". *Journal of Manufacturing Systems,* ***46***, pp. 272–281.
[28] Altenbach, H., Altenbach, J., Kissing, W., and Altenbach, H., 2004. *Mechanics of composite structural elements*. Springer.
[29] Jones, R. M., 1999. *Mechanics of composite materials*. CRC press.
[30] Nassar, S. A., and Abboud, A., 2009. "An Improved Stiffness Model for Bolted Joints". *Journal of Mechanical Design,* ***131***(12), 11. 121001.
[31] Olsson, A., Sandberg, G., and Dahlblom, O., 2003. "On latin hypercube sampling for structural reliability analysis". *Structural Safety,* ***25***(1), pp. 47–68.
[32] Yue, X., Wen, Y., Hunt, J. H., and Shi, J., 2020. "Active learning for gaussian process considering uncertainties with application to shape control of composite fuselage". *IEEE Transactions on Automation Science and Engineering,* ***18***(1), pp. 36–46.
[33] Lee, C., Wang, X., Wu, J., and Yue, X., 2021. "Failure-averse active learning for physics-constrained systems". *arXiv preprint arXiv:2110.14443*.
[34] Koenker, R., Chernozhukov, V., He, X., and Peng, L., 2017. *Handbook of quantile regression*. CRC press.
[35] De Haan, L., Ferreira, A., and Ferreira, A., 2006. *Extreme value theory: an introduction*, Vol. 21. Springer.
[36] Coles, S., Bawa, J., Trenner, L., and Dorazio, P., 2001. *An introduction to statistical modeling of extreme values*, Vol. 208. Springer.
[37] Kvam, P. H., and Vidakovic, B., 2007. *Nonparametric statistics with applications to science and engineering*, Vol. 653. John Wiley & Sons.
[38] Öner, M., and Deveci Kocakoç, İ., 2017. "A compilation of some popular goodness of fit tests for normal distribution: Their algorithms and MATLAB codes (matlab)". *Journal of Modern Applied Statistical Methods,* ***16***(2), p. 30.

Copyright © 2022 by ASME